Collectivity of nuclei near the exotic doubly magic ^{78}Ni by *ab initio* calculations

Z. C. Xu,[1] R. Z. Hu,[1] S. L. Jin,[1] J. H. Hou,[1] S. Zhang,[1] and F. R. Xu[1,2,*]

[1]*School of Physics, and State Key Laboratory of Nuclear Physics and Technology, Peking University, Beijing 100871, China*

[2]*Southern Center for Nuclear-Science Theory (SCNT), Institute of Modern Physics, Chinese Academy of Sciences, Huizhou 516000, China*

(Received 5 May 2024; accepted 24 July 2024; published 12 August 2024)

Neutron-rich nuclei are attracting significant attention due to vital roles in the nucleosynthesis processes of the universe. The shell evolution which breaks or creates magic numbers in some instances leads to shape coexistence that frequently serves as a portal to the islands of inversion (IOI). ^{74}Zn was suggested as a northern extension of the $N = 40$ IOI across $Z = 28$, and a new IOI around $N = 50$ ($Z = 20$–28) had also been predicted. We have performed *ab initio* calculations for even-even Zn isotopes and $N = 50$ ($Z > 28$) isotones located in the north of the $N = 40$ and 50 IOIs. With a chiral two- plus three-nucleon force, the shell-model valence-space effective Hamiltonian is derived using the many-body perturbation theory named $\hat{\mathrm{Q}}$-box folded diagrams, and the effective operators of electromagnetic transitions are obtained using similar $\hat{\Theta}$-box folded diagrams. The calculations reproduce experimental excitation energies and electric qudrupole transition strengths of excited states of the nuclei, showing a collectivity of $^{70\text{-}78}$Zn isotopes and a noncollectivity of the $N = 50$ ($Z > 28$) isotones.

DOI: 10.1103/PhysRevC.110.024308

I. INTRODUCTION

The abundances of chemical elements in the universe are a hot issue in nuclear astrophysics research. The rapid neutron capture (r-process) produces approximately half of the elements heavier than iron in the universe [1]. Therefore, studying the structure of neutron-rich nuclei is important for understanding nucleosynthesis processes [2]. The shell evolution in neutron-rich exotic nuclei, which breaks or creates magic numbers in some instances [3], leads to a distinctive manifestation of nuclear dynamics. This manifestation, rarely observed in interacting fermionic systems, is the phenomenon known as shape coexistence [4,5]. This phenomenon involves quantum states that exhibit distinct shapes while remaining close in energy. The energy difference frequently proves to be significantly smaller than those predicted by plain mean-field calculations in which the rotational symmetry is not conserved and configuration mixing is not considered. It has been shown that beyond-mean-field effects (e.g., from symmetry restoration and configuration mixing) can enhance the shape coexistence and significantly reduce the energy difference [6–9]. Shape coexistence in magic nuclei often serves as a portal to the islands of inversion (IOI) where a group of nuclei expected to be spherical in their ground states exhibits deformation instead.

Theoretical and experimental studies have unveiled the shape coexistence around ^{78}Ni [10–13]. This has also led to the theoretical prediction of the $N = 50$ IOI with deformed ground states in ^{76}Fe and ^{74}Cr by the large-scale shell model (LSSM) [14]. Recent experiments have suggested that ^{74}Zn acts as a northern extension of the $N = 40$ IOI across $Z = 28$, in which the ground state exhibits an enhanced axial-asymmetry shape (triaxiality) [15]. On the other hand, the collectivity or noncollectivity in $N = 50$ ($Z > 28$) isotones offers a special interest in understanding the northern edge of the $N = 50$ IOI.

In even-even nuclei, the excitation energy $E(2_1^+)$ of the first 2^+ excited state and the electric quadrupole transition strength $B(E2; 2_1^+ \to 0_1^+)$ serve as probes to the collectivity of the nucleus. The systematics of the collectivity in $E(2_1^+)$ and $B(E2; 2_1^+ \to 0_1^+)$ of Zn isotopes around $N = 40$ is similar to that of other $Z = 24$–36 isotopes except $Z = 28$, indicating that the $N = 40$ shell closure vanishes in the neutron-rich isotopes [16,17]. The $B(E2; 4_1^+ \to 2_1^+)/B(E2; 2_1^+ \to 0_1^+)$ ratio, also known as the B_{42} value, is another indicator of nuclear collectivity with a typical value of 1.5 for the collectivity [18].

The goal of *ab initio* calculations is to understand the structure of the nucleus from the underlying interaction among nucleons, with minimal reliance on experimental data beyond those essential to define nuclear forces. With the development of two- and three-nucleon forces (2NF and 3NF, respectively) from the chiral effective field theoy (χEFT) [19–22], *ab initio* many-body calculations have been playing important roles in many aspects of predicting the properties of nuclei, such as the location of the oxygen dripline [23–25], the Borromean structure of ^{17}Ne [26], and the origin of the anomalous long lifetime of ^{14}C [27]. A variety of observables for almost all open-shell nuclei accessible through the conventional shell model can be treated based on the *ab initio* many-body perturbation theory (MBPT) method [28,29]. The $\hat{\Theta}$-box method which uses the MBPT to derive valence-space effective operators of observables offers a powerful tool for the *ab initio* calculations of nuclear observables [30].

*Contact author: frxu@pku.edu.cn

In this work, based on χEFT forces, we have studied even-even Zn isotopes and $N = 50$ ($Z > 28$) isotones within the shell model with the valence-space effective Hamiltonian and other effective operators derived using the $\hat{Q}$- [31,32] and $\hat{\Theta}$-box folded diagrams [29,30,33], respectively. The neutron-rich Zn isotopes and $N = 50$ ($Z > 28$) isotones are located in the north of the $N = 40$ and 50 IOIs.

II. THE METHOD

Starting with the chiral 2NF plus 3NF, the intrinsic Hamiltonian of an A-nucleon system can be written as

$$H = \sum_{i=1}^{A}\left(1-\frac{1}{A}\right)\frac{p_i^2}{2m} + \sum_{i<j}^{A}\left(v_{ij}^{\mathrm{NN}} - \frac{\boldsymbol{p}_i\cdot\boldsymbol{p}_j}{mA}\right) + \sum_{i<j<k}^{A} v_{ijk}^{\mathrm{3N}}, \tag{1}$$

where $\boldsymbol{p}_i$ represents the nucleon momentum in the laboratory coordinates, m denotes the nucleon mass, and v^{NN} and v^{3N} correspond to 2NF and 3NF, respectively. The chiral 2NF plus 3NF labeled by EM1.8/2.0 [22] has been used. This interaction can globally reproduce nuclear binding energies [34,35].

For $Z = 30$ Zn isotopes and $N = 50$ isotones, we take ^{56}Ni as the core of the shell model and the reference state of the 3NF normal-ordered process. To include more correlations, we choose the Hartree-Fock (HF) single-particle states obtained with the same EM1.8/2.0 as the starting basis. The matrix elements of the interaction and other observable operator are transformed from the harmonic oscillator (HO) basis to the HF basis by computing overlaps between the HF and HO basis wave functions. Given the medium mass of the nuclei of interest, a large-space chiral interaction has been used with the HO basis at $\hbar\omega = 16$ MeV and covering 15 major shells (i.e., $e = 2n + l \leqslant e_{\max} = 14$). For 3NF, we limit $e_{3\max} = e_1 + e_2 + e_3 \leqslant 14$. The valence space of the shell model takes $\pi\{1p_{3/2}, 1p_{1/2}, 0f_{5/2}\}\otimes\nu\{1p_{3/2}, 1p_{1/2}, 0f_{5/2}, 0g_{9/2}, 1d_{5/2}\}$. In many-body calculations, 3NF is usually normal-ordered relative to a reference state, resulting in normal-ordered zero-, one- and two-body terms with the residual three-body term being neglected [25,34–37].

The valence-particle effective Hamiltonian and effective operators are constructed with the MBPT [28,30]. The Hamiltonian is separated into a zero-order part, H_0, and a perturbative part, H_1,

$$H = H_0 + (H - H_0) = H_0 + H_1, \tag{2}$$

where H_0 represents the one-body part of the normal-ordered Hamiltonian, while H_1 is the residual two-body part including the normal-ordered 3NF at the two-body level [25,37].

In the shell-model calculation, valence single-particle energies and effective interaction matrix elements can be obtained using so-called $\hat{S}$-box [38] and $\hat{Q}$-box folded diagrams [31,32], respectively. The $\hat{S}$-box is by definition the one-body part of the $\hat{Q}$ box. For the cross-shell shell-model calculation in which single-particle orbitals are not degenerated, the extended Kuo-Krenciglowa solution [39,40] of the $\hat{S}$-box and $\hat{Q}$-box folded diagrams can be used to derive the valence-space effective Hamiltonian H_{eff} by iterating,

$$H_{\mathrm{eff}}^{(\kappa)} = PH_0P + \hat{Q}(\epsilon) + \sum_{n=1}^{\infty}\frac{1}{n!}\frac{d^n\hat{Q}(\epsilon)}{d\epsilon^n}\left\{H_{\mathrm{eff}}^{(\kappa-1)} - \epsilon\right\}^n, \tag{3}$$

where κ represents the κth iteration, and ϵ is the starting energy.

The $\hat{Q}$ box is defined as

$$\hat{Q}(\epsilon) = PH_1P + PH_1Q\frac{1}{\epsilon - QHQ}QH_1P, \tag{4}$$

with derivatives such as

$$\hat{Q}_n(\epsilon) = \frac{1}{n!}\frac{d^n\hat{Q}(\epsilon)}{d\epsilon^n}, \tag{5}$$

where P and Q represent the projection operators for the model space and its complementary space (i.e., the excluded space), respectively, with $P + Q = 1$. The $\hat{S}$-box and $\hat{Q}$-box calculations are approximated up to the third order. With these MBPT calculations, we have derived the effective Hamiltonian for the chosen valence space of $\pi\{1p_{3/2}1p_{1/2}0f_{5/2}\}\otimes\nu\{1p_{3/2}1p_{1/2}0f_{5/2}0g_{9/2}1d_{5/2}\}$ with the ^{56}Ni core.

For other observables, the bare operators require to be renormalized into the valence space, which can be achieved using the so-called $\hat{\Theta}$-box folded diagrams within the MBPT framework, similar to the $\hat{Q}$-box diagrams. A valence-space effective operator, denoted by Θ_{eff}, which takes into account the contribution from the excluded Q space, can be written as

$$\Theta_{\mathrm{eff}} = \sum_{\alpha,\beta}|\psi_\alpha\rangle\langle\tilde{\Psi}_\alpha|\Theta|\Psi_\beta\rangle\langle\tilde{\psi}_\beta|, \tag{6}$$

where the valence-space wave function $|\psi_\alpha\rangle$ obtained from diagonalizing H_{eff} is the projection of the full-space wave function $|\Psi_\alpha\rangle$ onto the valence space, i.e., $|\psi_\alpha\rangle = P|\Psi_\alpha\rangle$.

In the MBPT, the $\hat{\Theta}$ box is defined as [29,33]

$$\hat{\Theta}(\epsilon) = P\Theta P + P\Theta Q\frac{1}{\epsilon - QHQ}QH_1P \tag{7}$$

and

$$\hat{\Theta}(\epsilon_1;\epsilon_2) = PH_1Q\frac{1}{\epsilon_1 - QHQ}Q\Theta Q\frac{1}{\epsilon_2 - QHQ}QH_1P, \tag{8}$$

with their derivatives

$$\hat{\Theta}_n = \frac{1}{n!}\frac{d^n\hat{\Theta}(\epsilon)}{d\epsilon^n} \tag{9}$$

and

$$\hat{\Theta}_{mn} = \frac{1}{m!n!}\frac{d^m}{d\epsilon_1^m}\frac{d^n}{d\epsilon_2^n}\hat{\Theta}(\epsilon_1;\epsilon_2)\Big|_{\epsilon_1=\epsilon_2=\epsilon}. \tag{10}$$

With the identity $\hat{Q}\hat{Q}^{-1} = 1$, the final perturbative expansion of the effective operator Θ_{eff} can be expressed by the $\hat{Q}$ box and the $\hat{\Theta}$ box as

$$\begin{aligned}\Theta_{\mathrm{eff}} &= (P + \hat{Q}_1 + \hat{Q}_1\hat{Q}_1 + \hat{Q}_2\hat{Q} + \hat{Q}\hat{Q}_2 + \cdots)\hat{Q}\hat{Q}^{-1} \\ &\quad\times(\chi_0 + \chi_1 + \chi_2 + \cdots) \\ &= H_{\mathrm{eff}}\hat{Q}^{-1}(\chi_0 + \chi_1 + \chi_2 + \cdots),\end{aligned} \tag{11}$$

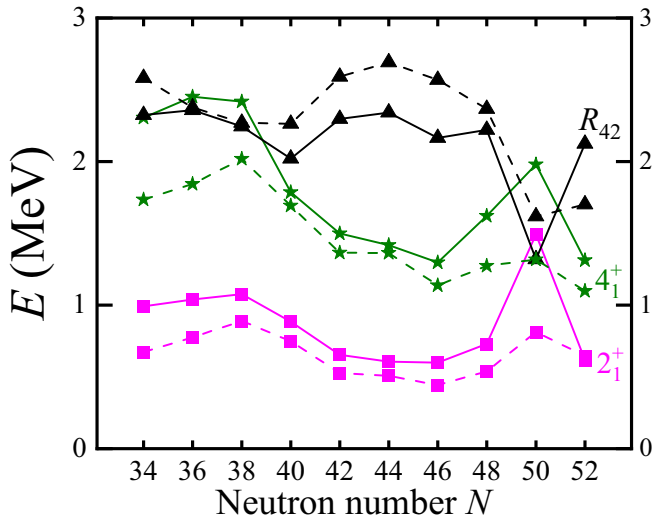

FIG. 1. Calculated (dashed lines) and experimental (solid lines) [17,42] excitation energies $E(2_1^+)$ (pink square) and $E(4_1^+)$ (cyan star) and their ratio $R_{42} = E(4_1^+)/E(2_1^+)$ (black triangle) in even-even Zn isotopes.

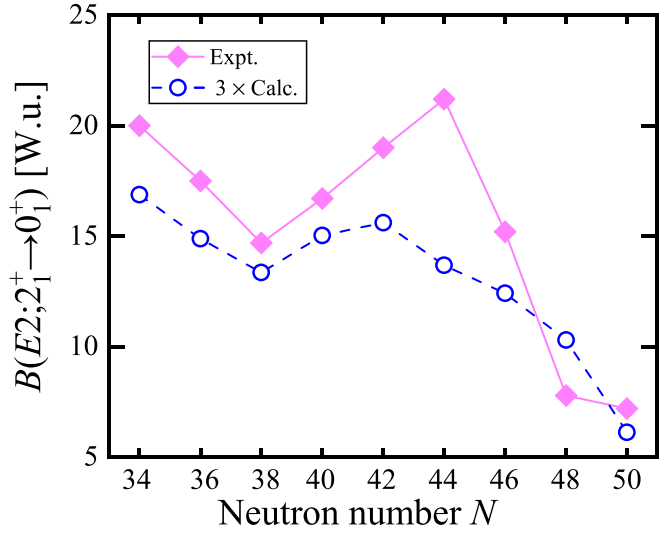

FIG. 2. Calculated and experimental [17,42] $B(E2; 2_1^+ \to 0_1^+)$ values in even-even Zn isotopes.

where χ_n is related to the $\hat{\Theta}$ box, the $\hat{Q}$ box, and their derivatives as

$$\begin{aligned}\chi_0 &= (\hat{\Theta}_0 + \text{H.c.}) + \hat{\Theta}_{00},\\ \chi_1 &= (\hat{\Theta}_1\hat{Q} + \text{H.c.}) + (\hat{\Theta}_{01}\hat{Q} + \text{H.c.}),\\ \chi_2 &= (\hat{\Theta}_1\hat{Q}_1\hat{Q} + \text{H.c.}) + (\hat{\Theta}_2\hat{Q}\hat{Q} + \text{H.c.})\\ &\quad + (\hat{\Theta}_{02}\hat{Q}\hat{Q} + \text{H.c.}) + \hat{Q}\hat{\Theta}_{11}\hat{Q}. \end{aligned} \tag{12}$$

In our calculations, the χ_n series are truncated up to the χ_2 order, which has been proved to be sufficient to obtain convergences [29]. The $\hat{\Theta}$ box is calculated up to the third order, which is consistent with the expansions used in the $\hat{S}$-box and $\hat{Q}$-box calculations.

In this study, we focus on the analysis of electromagnetic multipole transitions, characterized by the reduced transition probability given by

$$B(\sigma\lambda; \xi_i J_i \to \xi_f J_f) = \frac{1}{2J_i+1} |\langle \xi_f J_f \| \mathcal{M}_{\sigma\lambda} \| \xi_i J_i \rangle|^2, \tag{13}$$

where J_i and J_f represent the total angular momenta of the initial and final states, respectively, and ξ covers additional quantum numbers required to fully describe these states. The symbols $\sigma\lambda$ label the electric ($E\lambda$) or magnetic ($M\lambda$) multipoles. In this work, we focus on the $E2$ transition. The free-space bare $E2$-transition tensor operator is

$$\mathcal{M}_{E2} = \boldsymbol{Q}_2, \tag{14}$$

with the tensor components defined by

$$Q_{2\mu} = \sum_{j=1}^{A} e_j r_j^2 Y_{2\mu}(\hat{r}_j), \tag{15}$$

where e_j is the natural (bare) charge of the jth nucleon, i.e., $e = 1$ for the proton and $e = 0$ for the neutron.

In even-even nuclei, the ratio between $E2$-transition strengths can serve as an indicator for mapping the structure evolution from a noncollective seniority regime to a collective dynamics [18,41]:

$$B_{42} \equiv \frac{B(E2; 4_1^+ \to 2_1^+)}{B(E2; 2_1^+ \to 0_1^+)}. \tag{16}$$

It is a useful measurement to inspect how a nucleus is close to a closed shell, while it also offers insight into the underlying structure of the states [18].

III. CALCULATIONS AND DISCUSSIONS

As mentioned in Sec. I, ^{74}Zn was suggested as a northern extension of the $N = 40$ IOI across $Z = 28$ [15], and a further IOI around $N = 50$ was predicted by the LSSM calculation [14]. This raises an interesting question on the collectivity of $N = 50$ ($Z > 28$) isotones. Using the realistic shell model based on the chiral 2NF plus 3NF EM1.8/2.0, we have investigated $Z = 30$ Zn isotopes and $N = 50$ ($30 \leqslant Z \leqslant 36$) isotones.

Figure 1 shows the excitation energies of the first 2^+ and 4^+ states and their ratio $R_{42} = E(4_1^+)/E(2_1^+)$ in even-even Zn isotopes. The present calculations properly reproduce experimental data [17,42], showing a shell gap at the magic number of $N = 50$. Figure 2 presents calculated and experimental [17,42] $B(E2; 2_1^+ \to 0_1^+)$ values. Note that the calculated $B(E2)$ values are plotted by multiplying by a factor of 3. *Ab initio* calculations based on realistic nuclear forces usually give radii of nuclei smaller than those of experimental data [43], while the $B(E2)$ calculation is sensitive to the radius as seen in Eq. (15). In Ref. [44], using the EM1.8/2.0 interaction, calculations by *ab initio* valence-space in-medium similarity renormalization group give $B(E2)$ values smaller than those of experimental data. Missing correlations beyond the model space can also lead to a loss of the $E2$ strength in the calculation [45]. In phenomenological calculations, effective

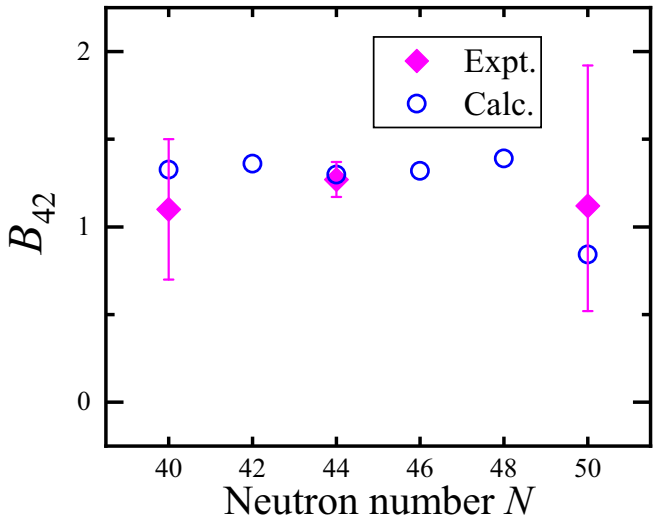

FIG. 3. Calculated and experimental [17,42] values of $B_{42} = B(E2; 4_1^+ \to 2_1^+)/B(E2; 2_1^+ \to 0_1^+)$ in the Zn isotopes of $40 \leqslant N \leqslant 50$.

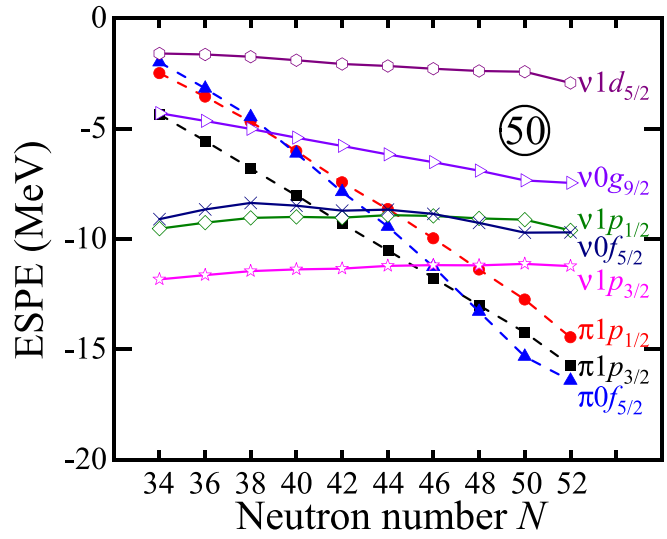

FIG. 4. Effective single-particle energies in the Zn isotopes, calculated with the EM1.8/2.0 interaction. The $N = 50$ neutron magic shell is clearly seen. Solid and dashed lines represent neutron (ν) and proton (π) orbitals, respectively.

charges determined by fitting data are usually used to give better quantitative descriptions of electric transition strengths.

Effective charges can be understood in the *ab initio* framework. As done in the present work using the $\hat{\Theta}$-box perturbation, in the *ab initio* calculation with a truncated model space, one needs to construct the model-space $E2$-transition effective operator starting from the bare $E2$ operator. The effective operator is eventually expressed by a matrix in correlated valence single-particle states $|\tilde{i}\rangle$ obtained, e.g., by the $\hat{S}$ box in this work. With the obtained effective operator matrix elements, one can define effective charges as [46,47]

$$e_{ij}^{\text{eff}} = e\frac{\langle\tilde{i}|\tilde{Q}_{2\mu}|\tilde{j}\rangle}{\langle i|Q_{2\mu}|j\rangle}, \tag{17}$$

where the numerator $\langle\tilde{i}|\tilde{Q}_{2\mu}|\tilde{j}\rangle$ is actually the $E2$ effective operator matrix elements (obtained by the $\hat{\Theta}$ box in this work), while the denominator $\langle i|Q_{2\mu}|j\rangle$ is simply calculated by the proton bare $E2$ operator in the uncorrelated (unperturbed) basis $|i\rangle$ (e.g., HO or HF basis). The $\hat{\Theta}$-box evolution of the $E2$ matrix from free space to valence space also results in a neutron $E2$ effective operator matrix similar to that of the proton. With the proton and neutron $E2$ effective operator matrices, we obtain the proton and neutron effective charges using Eq. (17). Therefore, in this picture, we can understand that effective charges result from the core polarization and virtual excitations to higher orbitals outside the model space [47]. Equation (17) shows that the matrix elements of the effective charges are orbital dependent. However, phenomenological shell-model calculations usually assume orbital-independent effective charges with the values determined by fitting experimental $E2$-transition strengths. In the *ab initio* calculation with the model space truncated, therefore, the valence effective operator is usually chosen without effective charges used. The effective charges are designed to play the similar role as the effective operator.

A decrease in $E(2_1^+)$ but an increase in $B(E2; 2_1^+ \to 0_1^+)$ indicates a collectivity of the nucleus. The systematics of $E(2_1^+)$ in Fig. 1 and $B(E2; 2_1^+ \to 0_1^+)$ in Fig. 2 in the Zn isotopes is similar to that in other $Z = 24 - 36$ isotopes (with an exception at $Z = 28$) [16,17], indicating that the $N = 40$ shell closure is weakened or even vanishes in the $Z = 24$–36 chains (except at the proton magic number of $Z = 28$) [16,17]. The present *ab initio* calculations give the consistent result.

The B_{42} ratios defined by Eq. (16) are presented in Fig. 3 for the Zn isotopes of $40 \leqslant N \leqslant 50$. We see that the present calculations well reproduce the data [17,42] within experimental error bars. It was mentioned in Ref. [18] that a collective motion of nucleus typically has a B_{42} value around 1.5. The present calculations give that the even-even $^{70\text{-}78}$Zn have their B_{42} values near 1.5, which is consistent with the collectivity in those nuclei. However, the situation is different in ^{80}Zn at $N = 50$, which we discuss later.

Calculating effective single-particle energies (ESPEs) [48] is useful to analyze the shell structure of nuclei. Figure 4 presents the ESPEs in the Zn isotopes. The $N = 50$ shell clearly appears. The $N = 40$ shell gap between $0g_{9/2}$ and $1p_{1/2}0f_{5/2}$ is weakened with increasing the neutron number. The orbitals $\nu 1p_{1/2}$ and $\nu 0f_{5/2}$ are close to each other parallelly, which increases the configuration mixing involving these two orbitals in many-body calculations.

As seen in Fig. 4, the proton $0f_{5/2}$ orbit drops significantly as the neutron number increases, lower than the $\pi 1p_{3/2}$ orbital after $N = 46$. This is because of the tensor force. As the neutron occupation number in $\nu 0g_{9/2}$ increases, the tensor force attracts the $\pi 0f_{5/2}$ orbit more, and repulses the $\pi 0f_{7/2}$ orbit more, leading to the drop of the $\pi 0f_{5/2}$ orbit.

The LSSM calculation [14] with a phenomenological interaction obtained based on the CD-Bonn potential predicts a deformation region and a new IOI around $N = 50$. Indeed, the present *ab initio* calculations show the collectivity in the Zn

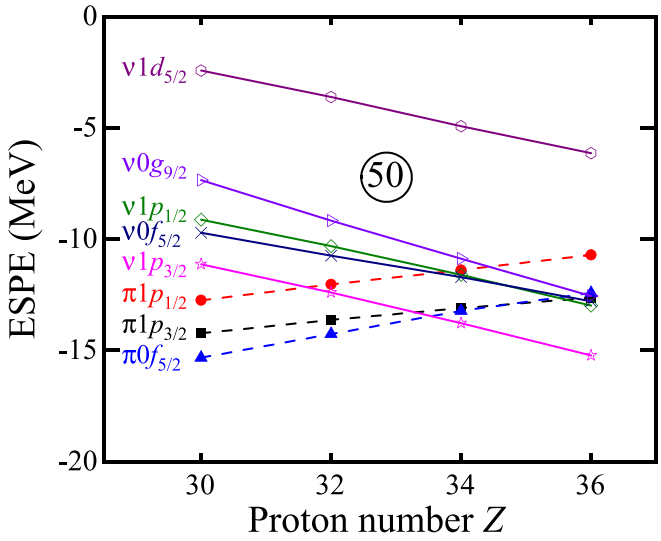

FIG. 5. Similar to Fig. 4, but for $N = 50$ isotones.

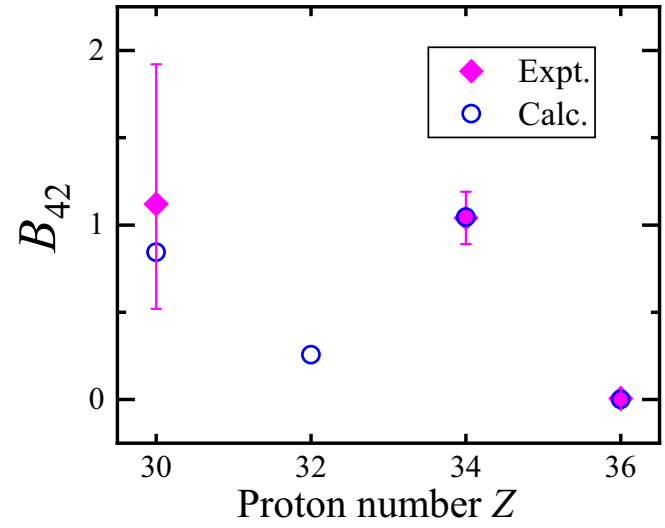

FIG. 6. Calculated and experimental [17,42] B_{42} values of the $N = 50$ isotones.

isotopes of $40 \leqslant N \leqslant 48$, exhibited through $E(2_1^+)$, $E(4_1^+)$, R_{42}, $B(E2)$, and B_{42} in Figs. 1–3. The collectivity had also been found in the $N = 50$ isotones with the proton numbers lower than the magic $Z = 28$, i.e., $20 \leqslant Z \leqslant 26$ [14].

With the ^{56}Ni core, we have also investigated the $N = 50$ ($Z = 30$–36) isotones heavier than the doubly magic isotone ^{78}Ni. Figure 5 displays the calculated ESPEs at $N = 50$. The $N = 50$ neutron magic shell between $\nu 1d_{5/2}$ and $\nu 0g_{9/2}$ is clearly seen in the $N = 50$ isotones. As mentioned, the B_{42} value is an indicator of the collectivity. Figure 6 displays the calculated B_{42} values of the $N = 50$ ($Z = 30$–36) isotones, compared with the data available, showing a noncollectivity in the $N = 50$ isotones heavier than ^{78}Ni. The noncollectivity indicates that the $N = 50$ IOI does not extend to the $Z > 28$ region.

IV. SUMMARY

We have performed *ab initio* calculations for the $Z = 30$ Zn isotopes located in the northwest of the exotic doubly magic nucleus ^{78}Ni and the $N = 50$ isotones in the north of ^{78}Ni. With a chiral two- plus three-nucleon force from the effective field theory, the cross-shell valence-space effective Hamiltonian and other effective operators were derived using the $\hat{\mathrm{Q}}$-box and $\hat{\Theta}$-box folded diagrams, respectively, with the ^{56}Ni core. As the main goal, we have investigated the collectivity or noncollectivity of nuclei in the ^{78}Ni region.

We focus on excitation spectra and electromagnetic transitions in the $Z = 30$ even-even Zn isotopes and $N = 50$ ($Z = 30$–36) isotones. The 2_1^+ and 4_1^+ excitation energies and their electric quadrupole transitions are good indicators of the collectivity. Our calculations reproduce reasonably experimental data for the neutron-rich nuclei. The systematics of $E(2_1^+)$, $E(4_1^+)/E(2_1^+)$, $B(E2; 2_1^+ \to 0_1^+)$, and $B(E2; 4_1^+ \to 2_1^+)/B(E2; 2_1^+ \to 0_1^+)$ in the Zn isotopes indicates a collectivity in $^{70\text{-}78}$Zn. The $N = 40$ shell closure that is usually thought to exist vanishes in the neutron-rich Zn isotopes, supported also by the calculations of effective single-particle energies. Calculations presented by the ratio of $B(E2; 4_1^+ \to 2_1^+)/B(E2; 2_1^+ \to 0_1^+)$ indicate a noncollectivity in the $N = 50$ isotones heavier than ^{78}Ni. Next to the discovered four islands of inversion located around $N = 8$, 20, 28, and 40, the large-scale shell-model calculations based on an phenomenological interaction predicted the fifth island of inversion around $N = 50$ ($20 \leqslant Z \leqslant 28$) [14]. The present *ab initio* calculations show that the $N = 50$ fifth island of inversion does not extend into the $Z > 28$ region.

ACKNOWLEDGMENTS

This work has been supported by the National Key R&D Program of China under Grant No. 2023YFA1606401 and the National Natural Science Foundation of China under Grants No. 12335007, No. 12035001, and No. 11921006. We acknowledge the High-Performance Computing Platform of Peking University for providing computational resources.

[1] F.-K. Thielemann, A. Arcones, R. Käppeli, M. Liebendörfer, T. Rauscher, C. Winteler, C. Fröhlich, I. Dillmann, T. Fischer, G. Martinez-Pinedo, K. Langanke, K. Farouqi, K.-L. Kratz, I. Panov, and I. K. Korneev, Prog. Part. Nucl. Phys. **66**, 346 (2011).

[2] R. N. Wolf, D. Beck, K. Blaum, C. Böhm, C. Borgmann, M. Breitenfeldt, N. Chamel, S. Goriely, F. Herfurth, M. Kowalska, S. Kreim, D. Lunney, V. Manea, E. Minaya Ramirez, S. Naimi, D. Neidherr, M. Rosenbusch, L. Schweikhard, J. Stanja, F. Wienholtz *et al.*, Phys. Rev. Lett. **110**, 041101 (2013).

[3] T. Otsuka, T. Matsuo, and D. Abe, Phys. Rev. Lett. **97**, 162501 (2006).
[4] P. E. Garrett, M. Zielińska, and E. Clément, Prog. Part. Nucl. Phys. **124**, 103931 (2022).
[5] K. Heyde and J. L. Wood, Rev. Mod. Phys. **83**, 1467 (2011).
[6] R. R. Rodríguez-Guzmán, J. L. Egido, and L. M. Robledo, Phys. Rev. C **62**, 054319 (2000).
[7] R. Rodríguez-Guzmán, J. L. Egido, and L. M. Robledo, Phys. Rev. C **65**, 024304 (2002).
[8] R. Rodríguez-Guzmán, J. Egido, and L. Robledo, Nucl. Phys. A **709**, 201 (2002).
[9] R. Rodríguez-Guzmán, J. Egido, and L. Robledo, Eur. Phys. J. A **17**, 37 (2003).
[10] K. Sieja and F. Nowacki, Phys. Rev. C **81**, 061303(R) (2010).
[11] K. Sieja and F. Nowacki, Phys. Rev. C **85**, 051301(R) (2012).
[12] A. Gottardo, D. Verney, C. Delafosse, F. Ibrahim, B. Roussière, C. Sotty, S. Roccia, C. Andreoiu, C. Costache, M.-C. Delattre, I. Deloncle, A. Etilé, S. Franchoo, C. Gaulard, J. Guillot, M. Lebois, M. MacCormick, N. Marginean, R. Marginean, I. Matea *et al.*, Phys. Rev. Lett. **116**, 182501 (2016).
[13] X. F. Yang, C. Wraith, L. Xie, C. Babcock, J. Billowes, M. L. Bissell, K. Blaum, B. Cheal, K. T. Flanagan, R. F. Garcia Ruiz, W. Gins, C. Gorges, L. K. Grob, H. Heylen, S. Kaufmann, M. Kowalska, J. Kraemer, S. Malbrunot-Ettenauer, R. Neugart, G. Neyens *et al.*, Phys. Rev. Lett. **116**, 182502 (2016).
[14] F. Nowacki, A. Poves, E. Caurier, and B. Bounthong, Phys. Rev. Lett. **117**, 272501 (2016).
[15] M. Rocchini, P. E. Garrett, M. Zielińska, S. M. Lenzi, D. D. Dao, F. Nowacki, V. Bildstein, A. D. MacLean, B. Olaizola, Z. T. Ahmed, C. Andreoiu, A. Babu, G. C. Ball, S. S. Bhattacharjee, H. Bidaman, C. Cheng, R. Coleman, I. Dillmann, A. B. Garnsworthy, S. Gillespie *et al.*, Phys. Rev. Lett. **130**, 122502 (2023).
[16] W. Rother, A. Dewald, H. Iwasaki, S. M. Lenzi, K. Starosta, D. Bazin, T. Baugher, B. A. Brown, H. L. Crawford, C. Fransen, A. Gade, T. N. Ginter, T. Glasmacher, G. F. Grinyer, M. Hackstein, G. Ilie, J. Jolie, S. McDaniel, D. Miller, P. Petkov *et al.*, Phys. Rev. Lett. **106**, 022502 (2011).
[17] https://www.nndc.bnl.gov/ensdf/.
[18] J. J. Ressler, R. F. Casten, N. V. Zamfir, C. W. Beausang, R. B. Cakirli, H. Ai, H. Amro, M. A. Caprio, A. A. Hecht, A. Heinz, S. D. Langdown, E. A. McCutchan, D. A. Meyer, C. Plettner, P. H. Regan, M. J. S. Sciacchitano, and A. D. Yamamoto, Phys. Rev. C **69**, 034317 (2004).
[19] E. Caurier, G. Martínez-Pinedo, F. Nowack, A. Poves, and A. P. Zuker, Rev. Mod. Phys. **77**, 427 (2005).
[20] R. Machleidt and D. Entem, Phys. Rep. **503**, 1 (2011).
[21] P. Navrátil, V. G. Gueorguiev, J. P. Vary, W. E. Ormand, and A. Nogga, Phys. Rev. Lett. **99**, 042501 (2007).
[22] K. Hebeler, S. K. Bogner, R. J. Furnstahl, A. Nogga, and A. Schwenk, Phys. Rev. C **83**, 031301(R) (2011).
[23] T. Otsuka, T. Suzuki, J. D. Holt, A. Schwenk, and Y. Akaishi, Phys. Rev. Lett. **105**, 032501 (2010).
[24] J. D. Holt, J. Menéndez, and A. Schwenk, Phys. Rev. Lett. **110**, 022502 (2013).
[25] S. Zhang, Y. Z. Ma, J. G. Li, B. S. Hu, Q. Yuan, Z. H. Cheng, and F. R. Xu, Phys. Lett. B **827**, 136958 (2022).
[26] Y. Z. Ma, F. R. Xu, N. Michel, S. Zhang, J. G. Li, B. S. Hu, L. Coraggio, N. Itaco, and A. Gargano, Phys. Lett. B **808**, 135673 (2020).
[27] P. Maris, J. P. Vary, P. Navrátil, W. E. Ormand, H. Nam, and D. J. Dean, Phys. Rev. Lett. **106**, 202502 (2011).
[28] T. T. S. Kuo, S. Y. Lee, and K. F. Ratcliff, Nucl. Phys. A **176**, 65 (1971).
[29] L. Coraggio and N. Itaco, Front. Phys. **8**, 345 (2020).
[30] Z. C. Xu, S. Zhang, J. G. Li, S. L. Jin, Q. Yuan, Z. H. Cheng, N. Michel, and F. R. Xu, Phys. Rev. C **108**, L031301 (2023).
[31] J. Shurpin, H. Müther, T. T. S. Kuo, and A. Faessler, Nucl. Phys. A **293**, 61 (1977).
[32] Z. H. Sun, Q. Wu, Z. H. Zhao, B. S. Hu, S. J. Dai, and F. R. Xu, Phys. Lett. B **769**, 227 (2017).
[33] K. Suzuki and R. Okamoto, Prog. Theor. Phys. **93**, 905 (1995).
[34] S. R. Stroberg, J. D. Holt, A. Schwenk, and J. Simonis, Phys. Rev. Lett. **126**, 022501 (2021).
[35] T. Miyagi, S. R. Stroberg, P. Navrátil, K. Hebeler, and J. D. Holt, Phys. Rev. C **105**, 014302 (2022).
[36] R. Roth, S. Binder, K. Vobig, A. Calci, J. Langhammer, and P. Navrátil, Phys. Rev. Lett. **109**, 052501 (2012).
[37] S. Zhang, F. R. Xu, J. G. Li, B. S. Hu, Z. H. Cheng, N. Michel, Y. Z. Ma, Q. Yuan, and Y. H. Zhang, Phys. Rev. C **108**, 064316 (2023).
[38] L. Coraggio and N. Itaco, Phys. Lett. B **616**, 43 (2005).
[39] K. Takayanagi, Nucl. Phys. A **852**, 61 (2011).
[40] N. Tsunoda, K. Takayanagi, M. Hjorth-Jensen, and T. Otsuka, Phys. Rev. C **89**, 024313 (2014).
[41] R. B. Cakirli, R. F. Casten, J. Jolie, and N. Warr, Phys. Rev. C **70**, 047302 (2004).
[42] Y. Shiga, K. Yoneda, D. Steppenbeck, N. Aoi, P. Doornenbal, J. Lee, H. Liu, M. Matsushita, S. Takeuchi, H. Wang, H. Baba, P. Bednarczyk, Z. Dombradi, Z. Fulop, S. Go, T. Hashimoto, M. Honma, E. Ideguchi, K. Ieki, K. Kobayashi *et al.*, Phys. Rev. C **93**, 024320 (2016).
[43] V. Somà, P. Navrátil, F. Raimondi, C. Barbieri, and T. Duguet, Phys. Rev. C **101**, 014318 (2020).
[44] N. M. Parzuchowski, S. R. Stroberg, P. Navrátil, H. Hergert, and S. K. Bogner, Phys. Rev. C **96**, 034324 (2017).
[45] S. R. Stroberg, J. Henderson, G. Hackman, P. Ruotsalainen, G. Hagen, and J. D. Holt, Phys. Rev. C **105**, 034333 (2022).
[46] P. J. Ellis and E. Osnes, Rev. Mod. Phys. **49**, 777 (1977).
[47] F. Raimondi and C. Barbieri, Phys. Rev. C **100**, 024317 (2019).
[48] Y. Z. Ma, L. Coraggio, L. De Angelis, T. Fukui, A. Gargano, N. Itaco, and F. R. Xu, Phys. Rev. C **100**, 034324 (2019).